Role of interfacial hydrophobicity in antimicrobial peptide magainin 2-induced nanopore formation

Role of Interfacial Hydrophobicity in Antimicrobial Peptide Magainin 2-induced Nanopore Formation

Moynul Hasan, [a,#] Farzana Hossain,[b] Hideo Dohra,[c,d] and Masahito Yamazaki [a, b, e, *]

[a] Integrated Bioscience Section, Graduate School of Science and Technology, Shizuoka University, Shizuoka, 422-8529, Japan

[b] Nanomaterials Research Division, Research Institute of Electronics, Shizuoka University, Shizuoka 422-8529, Japan

[c] Department of Science, Graduate School of Integrated Science and Technology, Shizuoka University, Shizuoka 422-8529, Japan.

[d] Instrumental Research Support Office, Research Institute of Green Science and Technology, Shizuoka 422-8529, Japan.

Present Address of Moynul Hasan – Department of Pharmacy, Jagannath University, Dhaka-1100, Bangladesh.

Corresponding Author

Masahito Yamazaki

Nanomaterials Research Division, Research Institute of Electronics, Shizuoka University, 836 Oya, Suruga-ku, Shizuoka 422-8529, Japan.

Email: yamazaki.masahito@shizuoka.ac.jp. FAX: 81-54-238-4741.

ABSTRACT

Antimicrobial peptide magainin 2 (Mag) forms nanopores in lipid bilayers and induces membrane permeation of the internal contents from vesicles. The binding of Mag to the membrane interface of a giant unilamellar vesicle (GUV) increases its fractional area change, δ, which is one of the main causes of Mag-induced nanopore formation. However, the role of its amino acid composition in the Mag-induced area increase and the following nanopore formation is not well understood. Here, to elucidate it we examined the role of interfacial hydrophobicity of Mag in its nanopore formation activity by investigating *de novo*-designed Mag mutants-induced nanopore formation in GUVs. Aligned amino acid residues in the α-helix of Mag were replaced to create 3 mutants: F5A-Mag, A9F-Mag, and F5,12,16A-Mag. These mutants have different interfacial hydrophobicity due to the variation of the numbers of Phe and Ala because the interfacial hydrophobicity of Phe is higher than that of Ala. The rate constant of Mag mutant-induced nanopore formation, k_p, increased with increasing numbers of Phe residues at the same peptide concentration. Further, the Mag mutant-induced δ increased with increasing numbers of Phe residues at the same peptide concentration. These results indicate that k_p and δ increase with increasing interfacial hydrophobicity of Mag mutants. The relationship between k_p and δ in the Mag and its mutants clearly indicates that k_p increases with increasing δ, irrespective of the difference in mutants. Based on these results, we can conclude that the interfacial hydrophobicity of Mag plays an important role in its nanopore formation activity.

Key words: antimicrobial peptide, nanopore formation, leakage, interfacial hydrophobicity, stretching of lipid bilayers, single GUV method

1. Introduction

In the past few decades, the number of multidrug-resistant (MDR) bacteria has increased [1,2], and thus, it is indispensable to develop new antibiotics. In this context, an emerging class of molecules called antimicrobial peptides (AMPs) that are produced by virtually all living organisms–mammals, animals, insects, and plants, have been defending their hosts against a variety of bacteria as well as other pathogenic microbes for millions of years [3-10]. Therefore, these AMPs have been considered as potential antibiotics against these MDR-bacteria [6,11,12]. Currently more than 3000 AMPs are known [13], and the antimicrobial and bactericidal activities of these AMPs are manifested through a variety of mode of actions [3-10]. Most AMPs induce leakage of internal contents from the cytoplasm of bacterial cells by damaging to their plasma membrane, which is considered a main cause of their bactericidal activity [3-10]. The lipid bilayer region of the plasma membrane is the main target of AMPs, as all D-amino acid AMPs exhibited similar activity to the wild-type (L-amino acid) AMPs [14]. On the other hand, some AMPs [15,16] have the same activities as cell-penetrating peptides (CPPs) [17-20], and thus, they can enter bacterial cytosol without inducing significant cytoplasmic leakage. It is considered that such CPP-type AMPs binds to DNA and/or proteins in the bacterial cytoplasm, which is considered the main mechanism of their bactericidal activities [21]. To reveal the mechanisms of action of AMPs and their design principles, their structure-function relationship study should be performed. Therefore, it is indispensable to develop various mutants of AMPs by changing multiple physicochemical parameters.

Magainin 2 (Mag) produced by the African clawed frog *Xenopus laevis* [22] is one of these AMPs and has been extensively examined. NMR spectroscopy revealed that Mag forms an α-helix in the membrane interface and orients parallel with the membrane surface [23,24]. Mag induces leakage of the internal contents from large unilamellar vesicles (LUVs) and giant unilamellar vesicles (GUVs) [25-27] following the formation of nanometer-size pores (i.e., nanopores) in the lipid bilayer [26]. It is considered that positively charged Mag binds to lipid bilayers due to electrostatic interactions and hydrophobic interaction [28,29]. With an increase in surface charge density, the apparent binding

constant of Mag to negatively charged GUVs increases, which enhance the rate constant of Mag-induced nanopore formation, k_p, in these lipid bilayers [30].

Recently, we have found that Mag locates in the outer leaflet of GUVs just before nanopore formation and the binding of Mag to the outer leaflet of a GUV increases the area of the lipid bilayer of the GUV, or the fractional area change of the GUV membrane, δ [31]. This, in combination with the relationship between k_p and Mag concentration in the membrane interface (surface concentration), one can reasonably conclude that k_p increases with increasing δ, i.e., the stretching of lipid bilayer activates Mag-induced nanopore formation [31,32]. At present, the mechanism of the Mag binding-induced area increase of the lipid bilayer is unknown. We have a following hypothesis on this mechanism. First, Mag binds with the lipid bilayer as a result of electrostatic attraction between the positively charged Mag and the negatively charged lipid membrane, which may decrease the area of the membrane due to the neutralization of the surface charges. Then, Mag is inserted deeply into the membrane interface because of the interfacial hydrophobicity of the hydrophobic side of the amphipathic α-helix. This last step increases the membrane area because of steric repulsion between the lipid headgroup and the rod-like structure of the α-helix. It is well recognized that the membrane interface of lipid bilayers in the liquid-crystalline phase is composed of hydrophilic segments and hydrocarbon chains of lipids and water [33,34] due to large thermal motions of lipids and lipid bilayers such as undulation and protrusion [35]. Thus, some amino acid residues favor in partitioning into the membrane interface. This tendency is characterized by the interfacial hydrophobicity of amino acids, which is defined as the transfer free energy of amino acid residue from bilayer interface to water, ΔG_{tr} [36]. Among 20 amino acid residues, Trp and Phe residues have the highest interfacial hydrophobicity. Thus, we can reasonably infer that an important factor in the insertion of peptides into the membrane interface is the interfacial hydrophobicity of their amino acid residues [37]. Mag (GIGKFLHSAKKFGKAFVGEIMNS-NH_2) has three Phe residues; thus, it can be predicted that Phe residues play an important role in the insertion of Mag into the membrane interface.

To reveal one of the design principles of Mag, we examined in this report the role of interfacial hydrophobicity of Mag in induced area increase of lipid bilayers and the following nanopore formation. For this purpose, we designed and synthesized several Mag mutants with different numbers of Phe residues by replacing Ala with Phe or Phe with Ala. Three Phe residues (F5, F12, F16) and an Ala residue (A9) are aligned along the hydrophobic side of the amphipathic α-helix. To maintain the secondary structure of Mag, we replaced the amino acid residues in this line to create 3 mutants: F5A-Mag, A9F-Mag, and F5,12,16A-Mag. The interfacial hydrophobicity of Phe (ΔG_{tr} = 4.7 kJ/mol) is higher than that of Ala (ΔG_{tr} = –0.7 kJ/mol). Thus, replacement of an Ala residue with a Phe residue of a peptide increases the interfacial hydrophobicity of the peptide by 5.4 kJ/mol. Accordingly, the interfacial hydrophobicity of A9F-Mag is higher than that of wild-type Mag by 5.4 kJ/mol. Oppositely, the interfacial hydrophobicity of F5A-Mag and F5,12,16A-Mag is lower than that of Mag by 5.4 kJ/mol and 16 kJ/mol, respectively. Thus, the order of interfacial hydrophobicity (from highest to lowest) is A9F-Mag > Mag > F5A-Mag > F5,12,16A-Mag. We investigated the Mag mutants-induced nanopore formation using the single GUV method [30,32]. We also examined the area change of GUV membranes induced by Mag mutants using two-micropipette method [31]. Based on these results, we discuss the role of interfacial hydrophobicity of Mag in area increase of lipid bilayers and nanopore formation.

2. Materials and Methods

2.1. Chemicals and peptides

Dioleoylphosphatidylglycerol (DOPG) and dioleoylphosphatidylcholine (DOPC) were purchased from Avanti Polar Lipids Inc. (Alabaster, AL, USA). Bovine serum albumin was purchased from Wako Pure Chemical Industry Ltd. (Osaka, Japan). Mag and its mutants (A9F-Mag, F5A-Mag, and F5,12,16A-Mag) were synthesized by the FastMoc method using a 433A peptide synthesizer (PE Applied Biosystems, Foster City, CA, USA), subsequently purified using reverse-phase high-performance liquid chromatography (HPLC) [26]. These peptides were also synthesized using an

Initiator+Alstra (Biotage, Uppsala, Sweden) [38]. Mass spectra of A9F-Mag, F5A-Mag, and F5,12,16A-Mag were acquired by LC−MS analysis using the linear ion trap time-of-flight mass spectrometer (LIT–TOF MS), NanoFrontier eLD (Hitachi High-Tech Corporation, Tokyo, Japan) coupled to a nanoflow HPLC, NanoFrontier nLC (Hitachi High-Tech Corporation, Tokyo, Japan) as previously described [39]. The measured masses of A9F-magainin, F5A-Mag, and F5,12,16A-Mag were 2540.4 ± 0.1, 2388.4 ± 0.1, and 2236.2 ± 0.1 Da, respectively, which correspond to the molecular masses calculated from the monoisotopic mass of all the atoms in these molecules.

Peptides were analyzed and purified by reverse-phase HPLC (LC-10AD and SPD-10A, Shimazu, Kyoto, Japan) using a C18 analytical column (4.6 × 250 mm, 5 μm) (Nakarai, Kyoto, Japan) and a C18 semi-preparative column (10 × 250 mm, 10 μm) (Nakarai), respectively. Solvent A (0.1 % trifluoroacetic acid in Milli-Q) and solvent B (0.1 % trifluoroacetic acid in 90% acetonitrile and 10% Milli-Q mixture) were used. For analysis of peptides, the initial solvent B (90% acetonitrile and 10% water) concentration in the mixture was 20% and the solvent B concentration increased linearly from 20% at 0 min to 50% at 60 min with a gradient of 0.5% solvent B/min.

2.2. GUV preparation and purification

GUVs comprising DOPG and DOPC (4/6; molar ratio) (i.e., DOPG/DOPC (4/6)-GUVs) were prepared by the natural swelling method [26,40]. Briefly, after prehydration of a dry DOPG/DOPC membrane, 1 mL of buffer A (10 mM PIPES, pH 7.0, 150 mM NaCl, and 1 mM EGTA) containing 0.10 M sucrose was added on the prehydrated membrane and then incubated for 2 h at 37 °C. We purified the GUVs using the standard membrane filtering method [40].

2.3. Mag mutant-induced nanopore formation in single GUVs

The single GUV method [30-32] was used to determine the rate constant of Mag mutant-induced nanopore formation. Briefly, the interaction of Mag mutant solution with single DOPG/DOPC (4/6)-

GUVs containing a water-soluble fluorescent probe, calcein, was observed in a hand-made microchamber whose glass surfaces were pre-coated with BSA under a fluorescent microscope (IX-70, Olympus, Tokyo, Japan) at 25 ± 1 °C (controlled using a stage thermocontrol system (Thermoplate, Tokai Hit, Shizuoka, Japan)). During the interaction of Mag mutants, GUV images were recorded using an EM-CCD camera (C9100-12, Hamamatsu Photonics K.K., Hamamatsu, Japan). To prevent the photobleaching of calcein, the incident light intensity was decreased by ND filters. The fluorescence intensity of each GUV lumen (I) was determined using an AquaCosmos (Hamamatsu Photonics K.K.). To induce the interaction of Mag mutants with single GUVs, Mag mutant solution in buffer A containing 0.10 M glucose were continuously added to the neighborhood of a GUV through a 20-μm-diameter micropipette located at the distance of 70 μm from the target GUV by applying a positive pressure of 30 Pa. Mag concentrations in the vicinity of a target GUV were 78% of those in the micropipette [31].

2.4. Mag mutant-induced area change of a GUV

We used a two-micropipette method to estimate the Mag mutant-induced area change of a GUV [31]. Under a DIC microscope (IX-71, Olympus), a single GUV was held in a chamber at the tip of micropipette with 10-μm-diameter for a few minutes by applying a slight aspiration pressure ΔP (to induce a membrane tension, σ, of 0.50 mN/m in the GUV). σ can be controlled by ΔP using a following equation.

$$\sigma = \frac{\Delta P d_{\mathrm{m}}}{4(1 - d_{\mathrm{m}}/D_{\mathrm{V}})} \qquad (1)$$

where d_{m} is the micropipette internal diameter and D_{V} is the diameter of the spherical part of the GUV outside the micropipette. Then, a Mag mutant solution was continuously added to the neighborhood of the GUV from another micropipette with 20-μm-diameter located at the distance of 40 μm from the target GUV by applying a positive pressure of 30 Pa. Mag mutant concentrations in the vicinity of the target GUV were 58% of those in the micropipette [31].

The fractional change in the area of a GUV membrane (δ) induced by the interaction of Mag mutants with the GUV is determined by the change in the projection length (ΔL) of a part of the GUV inside the micropipette. By assuming constant volume of a GUV, δ) is determined by ΔL as follows [41]:

$$\delta = \frac{\Delta L d_{\mathrm{p}}\left(1 - d_p/D_v\right)}{D_{\mathrm{v0}}^2} \qquad (2)$$

where D_{V} and D_{V0} are the diameter of the spherical part of the GUV outside the micropipette at equilibrium after and before the interaction with Mag mutant, respectively.

3. Results and Discussions

3. 1. Interfacial hydrophobicity of Mag mutants

In the reverse-phase HPLC, peptides are injected in a solvent containing high concentration of water and thus they are adsorbed in the hydrophobic surface of the resin, and then as the concentration of solvent B (hydrophobic solvent; here 90% acetonitrile/10% water was used) increases, the peptides are unbound from the resin to be eluted. Thus, the elution time of peptides or the corresponding solvent B concentration provides information of the hydrophobicity of the peptide. Figure 1 shows the elution pattern of the reverse phase-HPLC for purified Mag mutants. A9F-Mag was eluted at 43.5% solvent B, which was higher than that where Mag was eluted (40.5%), indicating that A9F-Mag is more hydrophobic than Mag. In contrast, F5A-Mag and F5,12,16A-Mag were eluted at 37.5% and 31.5% solvent B, respectively, which were lower than that where Mag was eluted (40.5%). This result indicates that F5A-Mag and F5,12,16A-Mag are more hydrophilic than Mag. Therefore, the order of the hydrophobicity of peptides (from highest to lowest) was A9F-Mag > Mag > F5A-Mag > F5,12,16A-Mag, which is the same order of the interfacial hydrophobicity of these Mag mutants described in the Introduction. Therefore, this result supports the above estimation of the interfacial hydrophobicity of these Mag mutants.

3.2. Mag mutants-induced nanopore formation in single GUVs

First, we examined the interaction of F5A-Mag with single DOPG/DOPC (4/6)-GUVs in PIPES buffer containing 0.10 M glucose at 25°C using the single GUV method. The GUVs contained a water-soluble fluorescent probe calcein in their lumen. Figure 2A shows a typical result for the interaction of 62 μM F5A-Mag with a single GUV. The phase-contrast microscopic image of a GUV before the interaction with F5A-Mag shows its high contrast (Fig. 2A (I)), attributed to the difference in refractive index between the inside (0.10 M sucrose) and the outside (0.10 M glucose) of the GUV. A fluorescence microscopic image of the same GUV (Fig. 2A (II)) showed high fluorescence intensity (I) of the GUV lumen due to a high calcein concentration there. In the interaction of the GUV with the peptide, I remained almost constant over the first 218 s, and then gradually decreased (Fig. 2A (II)). Figure 2B shows the time course of normalized I, defined as the ratio of $I(t)/I(0)$), where $I(t)$ and $I(0)$ are I at time t after starting the interaction and I before the interaction, respectively. After 360 s, $I(t)$ decreased to less than 20% of $I(0)$; however, a phase-contrast image of the same GUV (Fig. 2A (III)) showed a spherical GUV with a similar diameter. As discussed previously [26,30], the decrease in $I(t)$ is due to calcein leakage from the GUV lumen to the outside, indicating that F5A-Mag induced nanopores in the GUV membrane. Thus, the starting time of the decrease in $I(t)$ corresponds to the onset of nanopore formation in the lipid bilayer. After the same experiments were repeated using 20 single GUVs, we found that the calcein leakage from a GUV was initiated stochastically, indicating that nanopore formation occurred stochastically. To estimate the rate constant of nanopore formation at its initial stage, we obtained the time course of the fraction of intact GUV with no leakage of calcein among all examined GUVs, $P_{\mathrm{intact}}(t)$. If we consider a two-state transition from the intact state to the initial nanopore state, a following theoretical equation of P_{intact} is obtained [30,32],

$$P_{\mathrm{intact}}(t) = \exp\{-k_{\mathrm{r}}(t - t_{\mathrm{eq}})\} \qquad (3)$$

where k_{P} is the rate constant of the two-state transition, i.e., the rate constant of peptide-induced nanopore formation at its initial stage, and t_{eq} is a fitting parameter. Figure 2C shows that the time course

of P_{intact} for the interaction of 62 μM F5A-Mag was fit by Eq. 3, yielding a k_p value of 2.4×10^{-3} s^{-1}. Three independent experiments ($N = 3$) were carried out to obtain a mean value ± standard deviations (SDs) for k_P, $(2.3 \pm 0.2) \times 10^{-3}$ s^{-1}. The k_P increased with an increase in F5A-Mag concentration (Fig. 2D). The values of k_P for F5A-Mag were smaller than those of Mag at similar concentrations.

Second, we investigated A9F-Mag-induced calcein leakage from single GUVs. Figure 3A shows a typical result for the interaction of 10 μM A9F-Mag with a single GUV. Almost constant I was observed over the first 174 s of the interaction, then $I(t)$ decreased gradually, and at 360 s, $I(t)$ was almost zero (Fig. 3B). The time course of the decrease in P_{intact} was fit by a single exponential curve of Eq. 3 (Fig. 3C), yielding a k_p value of 4.5×10^{-3} s^{-1}. The mean ± SD value of k_P for 10 μM A9F-Mag was $(4.7 \pm 0.4) \times 10^{-3}$ s^{-1} ($N = 3$). The k_P increased with increasing A9F-Mag concentration, and the values of k_P for A9F-Mag were larger than those of Mag at similar concentrations (Fig. 3D).

Third, we investigated F5,12,16A-Mag-induced calcein leakage from single GUVs. F5,12,16A-Mag did not induce calcein leakage from the GUVs up to 62 μM, indicating no nanopore formation.

In summary, the results as a whole indicate that the rate constant of Mag mutants-induced nanopore formation, k_p, increases with increasing number of Phe residues at the same peptide concentration (Figs. 2D and 3D). Thus, the order of k_p of the Mag mutants at the same peptide concentration is A9F-Mag > Mag > F5A-Mag > F5,12,16A-Mag. This result indicates that k_p increases with increasing interfacial hydrophobicity of Mag mutants.

3.3. Mag mutants-induced area change of lipid bilayers

To reveal the mechanism of the effect of Mag mutation on nanopore formation, we examined the change in GUV area induced by Mag mutants using the two-micropipettes method [31]. First, we investigated the F5A-Mag-induced area change of a GUV. An F5A-Mag solution was continuously added to the vicinity of a single GUV held at the tip of micropipette A from micropipette B. After starting the interaction of F5A-Mag with the GUV, the fractional area change of the GUV, δ, increased

with time, and then reached an equilibrium value in less than 30 s (Fig. 4A). Figure 4B (●) shows that the value of δ at the equilibrium state increased with increasing F5A-Mag concentration in the buffer, and the values of δ for F5A-Mag were smaller than those for Mag (red ●) at similar concentrations. Next, we investigated the effects of A9F-Mag binding to the membrane of a GUV on its area using the same method as described above. The δ increased with time, and then reached an equilibrium value in less than 30 s. The values of δ for A9F-Mag (blue ▲) were larger than those for Mag at similar concentrations (Fig. 4B).

In summary, the order of the Mag mutant-induced δ at the same peptide concentration is A9F-Mag > Mag > F5A-Mag > F5,12,16A-Mag. This result indicates that δ increases with increasing interfacial hydrophobicity of Mag mutants.

3.4. Correlation between the rate constant of Mag mutants-induced nanopore formation and fractional area change

Figure 5 shows the relationship between the rate constant of nanopore formation, k_p, and the fractional area change, δ, induced by the three Mag mutants and Mag. The result shown in Fig. 5 demonstrates that k_p increases with increasing δ. This result is similar to the previous result, in which the rate constant of Mag-induced nanopore formation increases with increasing δ [31].

Based on this result, it can be reasonably explained that k_p increases with increasing interfacial hydrophobicity of Mag (ΔG_{tr}). The increase in ΔG_{tr} raises the binding constant of Mag to the GUV membrane interface, resulting in an increase in the Mag surface concentration, X. The insertion of amino acid residues such as Phe of Mag into the membrane interface can induce the repulsion between the headgroup of lipids and Mag, which increases the area of the lipid bilayer. The value of δ may depend on not only X but also the degree of insertion of Mag into the membrane interface, which depends on the interfacial hydrophobicity of Mag. Thus, δ increases with increasing the interfacial hydrophobicity of Mag. As described previously [31,32], the rate constant of Mag-induced nanopore formation in lipid

bilayers (k_p) increases with an increase in δ induced by the binding of Mag to the outer leaflet interface. The result of Fig. 5 supports that this mechanism is held for Mag mutants. Therefore, k_p increases with increasing interfacial hydrophobicity of Mag mutants.

4. Conclusions

In this report, to elucidate the role of the interfacial hydrophobicity of Mag in nanopore formation, we designed several Mag mutants with different numbers of Phe residues. The rate constant of Mag mutant-induced nanopore formation, k_p, in single GUVs and the fractional area change of the GUVs induced by Mag mutants, δ, increased with increasing number of Phe residues at the same peptide concentration, indicating that k_p and δ increase with increasing interfacial hydrophobicity of Mag mutants. These experimental results clearly indicate that the deep insertion of Mag into the membrane interface due to its interfacial hydrophobicity induces the increase in area of the GUV lipid bilayer. Based on these results, we concluded that as the interfacial hydrophobicity of Mag mutants increases, δ increases, and thus, k_p increases. This result provides a new design principle of AMPs, i.e., a clue of amino acid composition of Mag and other AMPs for their nanopore formation activity, and thus, is useful to design new AMPs.

Funding: Grants-in-Aid for Scientific Research (B) (No. 15H04361 and 19H03193) from the Japan Society for the Promotion of Science (JSPS) to M.Y. and the Cooperative Research Project of Research Center for Biomedical Engineering.

REFERENCES

(1) S.B. Levy, B. Marshall, Antibacterial resistance worldwide: causes, challenges and responses. Nature Medicine 10 (2004) S122-S129.

(2) K. Bush, P. Courvalin, C. Dantos, J. Davies, B. Eisenstein, P. Huovinen. G.A. Jacoby, R. Kishony, B.N. Kreiswirth, E. Kutter, S.A. Lerner, S. Levy, K. Lewis, O. Lomovskaya, J.H. Miller, S. Mpbashery, L.J.V. Piddock, S. Projan, C.M. Thomas, A. Tomasz, P.M. Tulkens, T.R. Waish, J.D. Watson, J. Witkovski, G.W. Wright, P. Yeh, H.I. Zgurskaya, Tacking antibiotic resistance. Nature Rev. Microbiol. 9 (2011) 894-896.

(3) P.M. Hwang, H.J. Vogel, Structure-function relationships of antimicrobial peptides. Biochem. Cell Biol. 76 (1998) 235-246.

(4) M. Zasloff, Antimicrobial peptides of multicellular organisms. Nature 415 (2002) 389-395.

(5) M.R. Yeaman, N.Y. Yount, Mechanisms of antimicrobial peptide action and resistance. Pharmaco. Rev. 55 (2003) 27-55.

(6) R.E.W. Hancock, S. Hans-Georg, Antimicrobial and host-defense peptides as new anti-infective therapeutic strategies. Nat. Biotech. 24 (2006)1551-1557.

(7) M.N. Melo, R. Ferre, A.R.B. Castanho, Antimicrobial peptides: linking partition, activity and high membrane-bound concentrations. Nat. Rev. Microbiol. 8 (2009) 1-5.

(8) K.A. Sochacki, K.J. Barns, R. Bucki, J.C. Weisshaar, Real-time attack on single Escherichia coli cells by the human antimicrobial peptide LL-37. Proc. Natl. Acad. Sci. U. S. A. 108 (2011) E77-E81.

(9) D.C. Propheter, A.L. Chara, T.A. Harris, K.A. Ruhn, L.V. Hooper, Resistin-like molecule β is a bactericidal protein that promotes spatial segregation of the microbiota and the colonic epithelium. Proc. Natl. Acad. Sci. U.S.A. 114 (2017) 11027-11033.

(10) K. Matsuzaki (ed), Antimicrobial Peptides: Basic for Clinical Application, Springer Nature, 2019.

(11) B.J. Brooks, A.E. Brooks, Therapeutic strategies to combat antibiotic resistance. Adv Drug Deli Rev 78 (2014) 14-27.

(12) F. Costa, C. Teixeira, P. Gomes, M.C.L. Martins, Clinical applications of AMPs, in: K. Matsuzaki (ed), Antimicrobial Peptides: Basic for Clinical Application, Springer Nature, Singapore. 2019, pp. 281-298.

(13) University of Nebraska Medical Center. Antimicrobial Peptide Database (APD3). https://aps.unmc.edu

(14) S. Bobone, L. Stella, Selectivity of antimicrobial peptides; a complex interplay of multiple equilibria, in: K. Matsuzaki (ed), Antimicrobial Peptides: Basic for Clinical Application, Springer Nature, Singapore. 2019, pp. 175-214.

(15) C.B. Park CB, K.-S. Yi, K. Matsuzaki, M.S. Kim, S.C. Kim, Structure-activity analysis of buforin II, a histone H2A-derived antimicrobial peptide: The proline hinge is responsible for the cell-penetrating ability of buforin II. Proc. Natl. Acad. Sci. U.S.A. 97 (2000) 8245-8250.

(16) F. Hossain, H. Dohra, M. Yamazaki, Effect of membrane potential on entry of lactoferricin B-derived 6-residue antimicrobial peptide into single *Escherichia coli* cells and lipid vesicles, J. Bacteriology, 203 (2021) e00021-21.

(17) M. Magzoub, A. Gräslund, Cell-penetrating peptides: small from inception to application. Quart. Rev. Biophys. 37 (2004) 147-195.

(18) M. Zorko, Ű. Langel, Cell-penetrating peptides: mechanism and kinetics of cargo delivery. Adv. Drug. Deliv. Rev. 57 (2005) 529-545.

(19) F. Madani, S. Lindberg, Ű. Langel, S. Futaki, A. Gräslund, Mechanisms of cellular uptake of cell-penetrating peptides. J. Biophysics. (2011) 414729.

(20) C. Bechara, S. Sagan, Cell-penetrating peptides: 20 years later, where do we stand? FEBS Lett. 587 (2013) 1693-1702.

(21) K.A. Brogden, Antimicrobial peptides: pore formers or metabolic inhibitors in bacteria? Nat Rev Microbiol 3 (2005) 238-250.

(22) M. Zasloff, Magainins, a class of antimicrobial peptides from Xenopus skin: Isolation, characterization of two active forms, and partial cDNA sequence of a precursor. Proc. Natl. Acad. Sci. U.S.A. 84 (1987) 5449-5453.

(23) B. Bechniger, M. Zasloff, S.J. Opella, Structure and orientation of the antibiotic peptide magainin in membranes by solid-state nuclear magnetic resonance spectroscopy. Protein. Sci. 2 (1993) 2077-2084.

(24) E. Strandberg, P. Tremouihac, P. Wadhwani, A.S. Ulrich, Synergetic transmembrane insertion of the heterodimeric PGLa/magainin 2 complex studied by solid-state NMR. Biochim. Biophys. Acta 1788 (2009) 1667-1679.

(25) K. Matsuzaki, O. Murase, N. Fujii, K. Miyajima, An antimicrobial peptide, magainin 2, induced rapid flip-flop of phospholipids coupled with pore formation and peptide translocation. Biochemistry 35 (1996) 11361-11368.

(26) Y. Tamba, M. Yamazaki, Single giant unilamellar vesicle method reveals effect of antimicrobial peptide Magainin 2 on membrane permeability. Biochemistry 44 (2005) 15823-15833.

(27) S.M. Gregory, A. Pokorny, P.F.F. Almeida, Magainin 2 revisited: a test of the quantitative model for the all-or-none permeabilization of phospholipid vesicles. Biophys. J. 96 (2009) 116-131.

(28) M.R. Wenk, J. Seelig, Magainin 2 amide interaction with lipid membranes: calorimetric detection of peptide binding and pore formation, Biochemistry, 37 (1998) 3909-3916.

(29) T. Wieprecht, O. Apostolov, J. Seelig, Binding of the antimicrobial peptide magainin 2 amide to small and large unilamellar vesicles, Biophys. Com. 85 (2000) 187-198.

(30) Y. Tamba, M. Yamazaki, Magainin 2-induced pore formation in membrane depends on its concentration in membrane interface. J. Phys. Chem. B 113 (2009) 4846-4852.

(31) M.A.S. Karal, J.M. Alam, T. Takahashi, V. Levadny, M. Yamazaki, Stretch-Activated pore of Antimicrobial Peptide Magainin 2. Langmuir 31 (2015) 3391-3401.

(32) M. Hasan, M.A.S. Karal, V. Levadnyy, M. Yamazaki, Mechanism of initial stage of pore formation induced by antimicrobial peptide magainin 2. Langmuir 34 (2018) 3349-3362.

(33) M.C. Wiener, S.H. White, Structure of a fluid dioleoylphosphatidylcholine bilayer determined by joint refinement of X-ray and neutron diffraction data. III. Complete structure, Biophys. J. 61 (1992) 434-447.

(34) S.H. White, W.C. Wimley, Peptide in lipid bilayers: structural and thermodynamic basis for partitioning and folding, Curr. Opin. Struct. Biol. 4 (1994) 79-86.

(35) J. Israerachvili, *Intermolecular & Surface Forces*, 2 nd ed. Academic Press, New York. 1992.

(36) W.C. Wimley, S.H. White, Experimentally determined hydrophobicity scale for proteins at membrane interface. Nature Struct. Biol. 3 (1996) 842-848.

(37) Y. Yamashita, S.M. Masum, T. Tanaka, M. Yamazaki, Shape changes of giant unilamellar vesicles of phosphatidylcholine induced by a de novo designed peptide interacting with their membrane interface. Langmuir, 18 (2002) 9638-9641.

(38) M.M. Or Rashid, M.M.R. Moghal, M.M. Billah, M. Hasan, M. Yamazaki, Effect of membrane potential on pore formation by the antimicrobial peptide magainin 2 in lipid bilayers. BBA-Biomembranes, 1862 (2020) 183381.

(39) M. Moniruzzaman, J.M. Alam, H. Dohra, M. Yamazaki, Antimicrobial peptide lactoferricin B-induced rapid leakage of internal contents from single giant unilamellar vesicles. Biochemistry 54 (2015) 5802-5814.

(40) Y. Tamba, H. Terashima, M. Yamazaki, A membrane filtering method for the purification of giant unilamellar vesicles. Chem. Phys. Lipids 164 (2011) 351-358.

(41) W. Rawictz, K.C. Olbrich, T. McIntosh, D. Needham, E. Evans, Effect of chain length and unsaturation on elasticity of lipid bilayers. Biophys. J. 79 (2000) 328-339.

Figure Legends

Figure 1. Reversed-phase HPLC chromatograms of Mag mutants. Solvent B (90% acetonitrile and 10% water) concentration in the mixture (broken line) was increased linearly from 20% at 0 min with a gradient of 0.5% solvent B/min. A9F-Mag (blue curve, A9F), Mag (red curve, WT (wild type)), F5A-Mag (black curve, F5A) and F5,12,16A-Mag (green curve, F5,12,16A). The absorbance of peptide solution at 215 nm is represented by arbitrary voltage.

Figure 2. F5A-Mag-induced nanopore formation in lipid bilayers. (A) Interaction of 62 μM F5A-Mag with a GUV containing calcein. (I) (III) phase contrast images of the GUV, and (II) its fluorescence microscopic images due to calcein. The numbers above each image show the time after an F5A-Mag solution was added to the neighborhood of the GUV. Bar, 30 μm. (B) Time course of normalized lumen intensity (I) shown in panel A. (C) Time course of P_{intact} in the interaction of 62 μM F5A-Mag. A red line is the best fit curve of Eq. 3. (D) Dependence of k_{P} on peptide concentration. F5A-Mag (●) and Mag (red ●). The mean values and SDs of k_{p} (N =3) are shown.

Figure 3. A9F-Mag-induced nanopore formation in lipid bilayers. (A) Interaction of 10 μM A9F-Mag with a GUV containing calcein. (I) (III) phase contrast images of the GUV, and (II) its fluorescence microscopic images due to calcein. The numbers above each image show the time after an A9F-Mag solution was added to the neighborhood of the GUV. Bar, 30 μm. (B) Time course of n normalized I shown in panel A. (C) Time course of P_{intact} in the interaction of 10 μM A9F-Mag. A red line is the best fit curve of Eq. 3. (D) Dependence of k_{P} on peptide concentration. A9F-Mag (blue ▲) and Mag (red ●). The mean values and SDs of k_{p} (N =3) are shown.

Figure 4. Mag mutants-induced area change of GUVs. (A) Time course of change in the fractional change in area, δ, of single GUVs interacting with F5A-Mag solution. The peptide concentration is denoted at the right side of each curve. (B) Dependence of δ at the equilibrium state on the mutant Mag concentration. A9F-Mag (blue ▲), Mag (red ●), F5A-Mag (●) and F5,12,16A-Mag (green ■).

Figure 5. The relationship between the rate constant of Mag mutants-induced nanopore formation, k_p, and the fractional area change, δ. A9F-Mag (blue ●), Mag (red ●), and F5A-Mag (●).

Figure 1

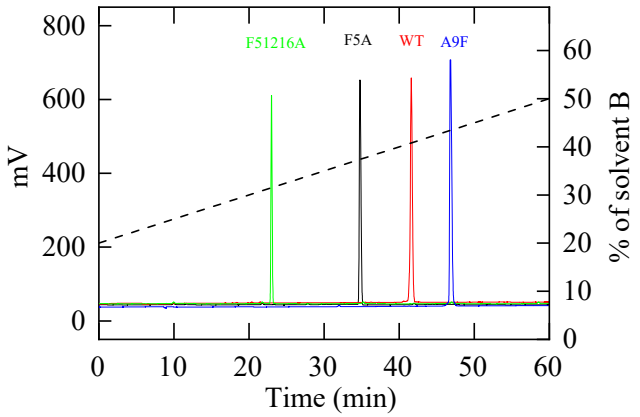

Figure 1. Reversed-phase HPLC chromatograms of Mag mutants. Solvent B (90% acetonitrile and 10% water) concentration in the mixture (broken line) was increased linearly from 20% at 0 min with a gradient of 0.5% solvent B/min. A9F-Mag (blue curve, A9F), Mag (red curve, WT (wild type)), F5A-Mag (black curve, F5A) and F5,12,16A-Mag (green curve, F5,12,16A). The absorbance of peptide solution at 215 nm is represented by arbitrary voltage.

Figure 2

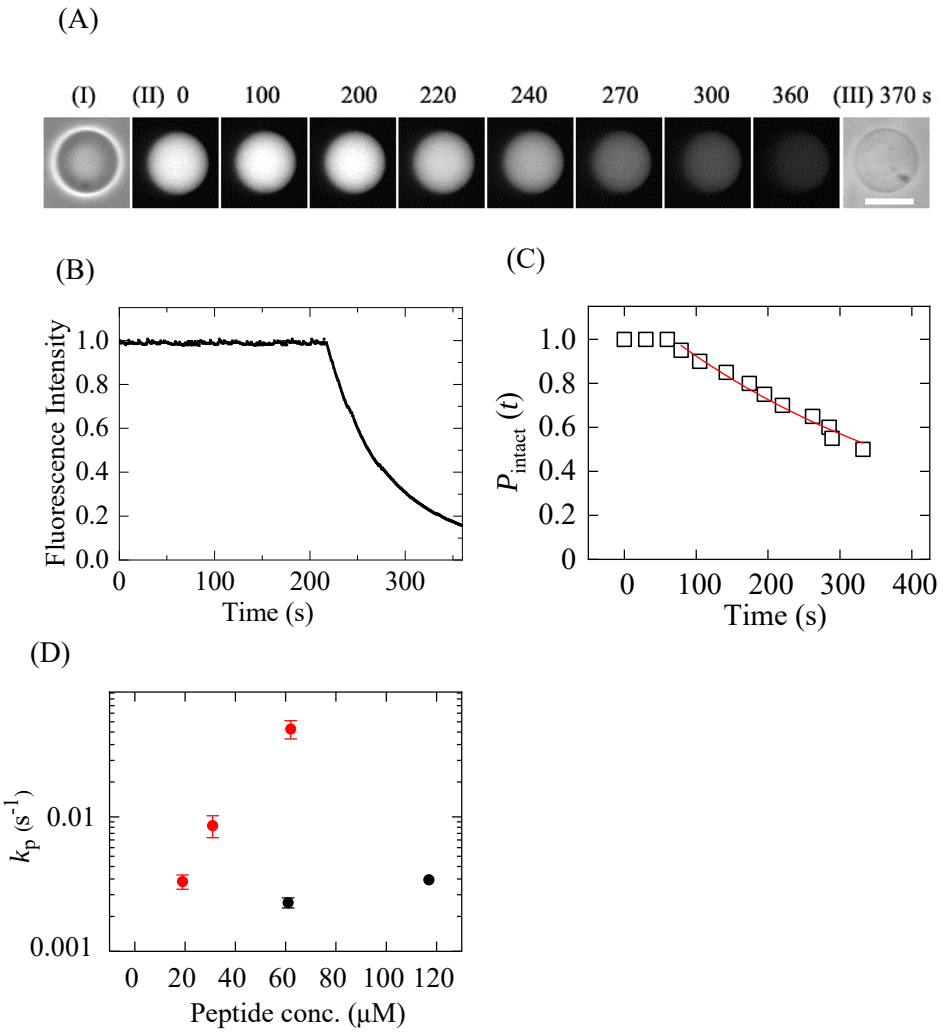

Figure 2. F5A-Mag-induced nanopore formation in lipid bilayers. (A) Interaction of 62 μM F5A-Mag with a GUV containing calcein. (I) (III) phase contrast images of the GUV, and (II) its fluorescence microscopic images due to calcein. The numbers above each image show the time after an F5A-Mag solution was added to the neighborhood of the GUV. Bar, 30 μm. (B) Time course of normalized lumen intensity (I) shown in panel A. (C) Time course of P_{intact} in the interaction of 62 μM F5A-Mag. A red line is the best fit curve of Eq. 3. (D) Dependence of k_P on peptide concentration. F5A-Mag (●) and Mag (red ●). The mean values and SDs of k_p (N =3) are shown.

Figure 3

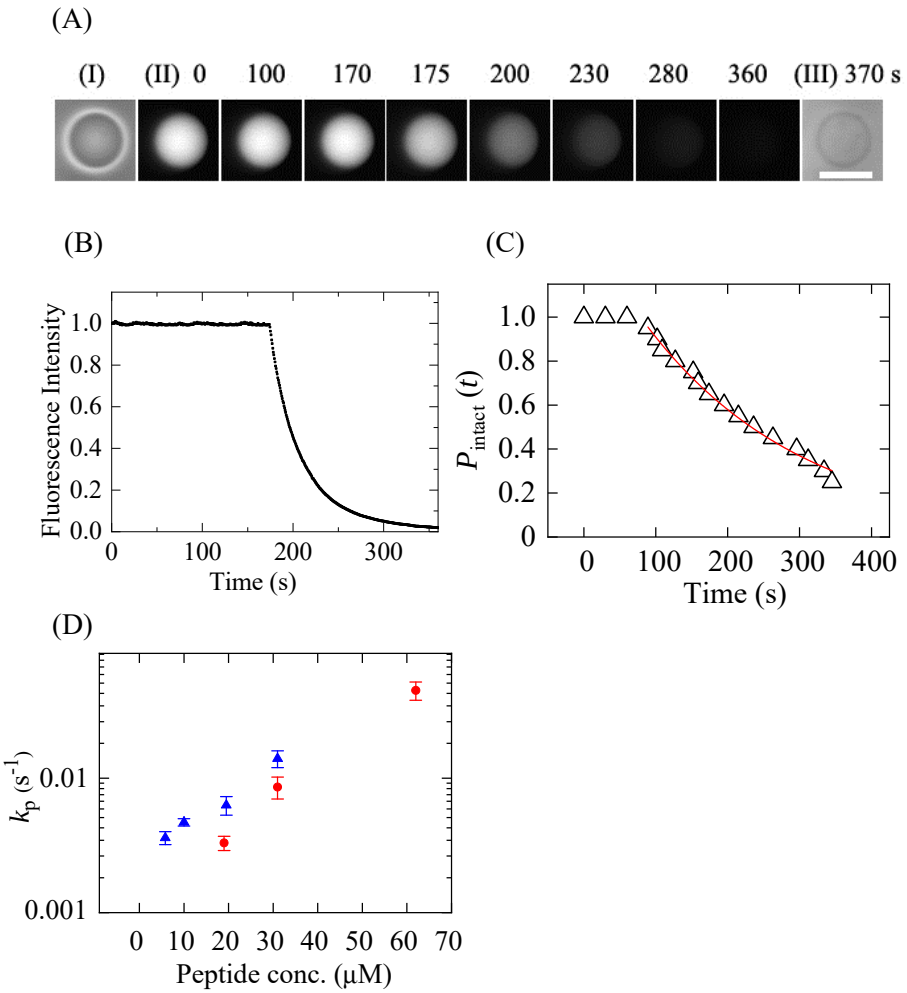

Figure 3. A9F-Mag-induced nanopore formation in lipid bilayers. (A) Interaction of 10 μM A9F-Mag with a GUV containing calcein. (I) (III) phase contrast images of the GUV, and (II) its fluorescence microscopic images due to calcein. The numbers above each image show the time after an A9F-Mag solution was added to the neighborhood of the GUV. Bar, 30 μm. (B) Time course of n normalized I shown in panel A. (C) Time course of P_{intact} in the interaction of 10 μM A9F-Mag. A red line is the best fit curve of Eq. 3. (D) Dependence of k_P on peptide concentration. A9F-Mag (blue ▲) and Mag (red ●). The mean values and SDs of k_p (N =3) are shown.

Figure 4

(A)

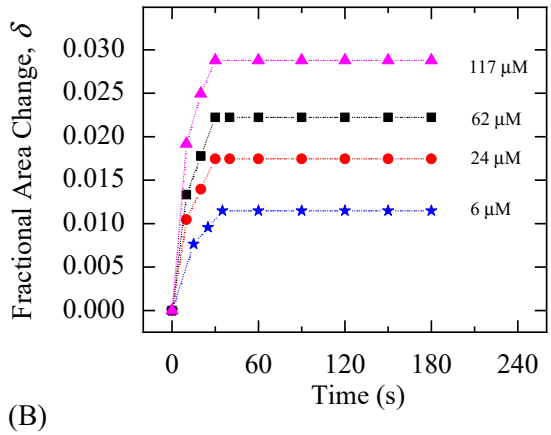

(B)

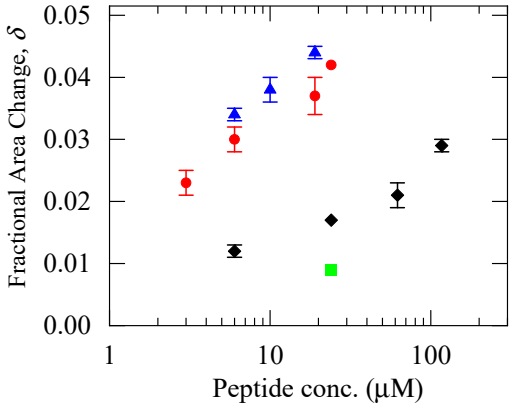

Figure 4. Mag mutants-induced area change of GUVs. (A) Time course of change in the fractional change in area, δ, of single GUVs interacting with F5A-Mag solution. The peptide concentration is denoted at the right side of each curve. (B) Dependence of δ at the equilibrium state on the mutant Mag concentration. A9F-Mag (blue ▲), Mag (red ●), F5A-Mag (●) and F5,12,16A-Mag (green ■).

Figure 5

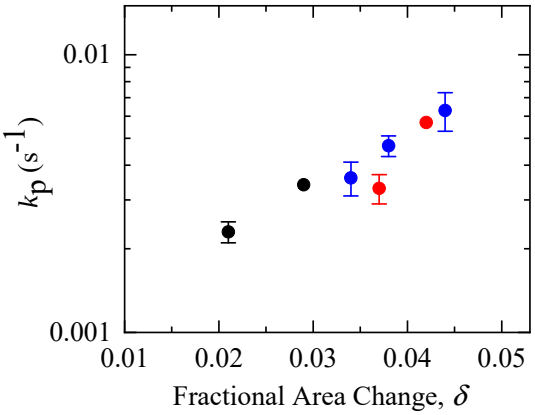

Figure 5. The relationship between the rate constant of Mag mutants-induced nanopore formation, k_p, and the fractional area change, δ. A9F-Mag (blue ●), Mag (red ●), and F5A-Mag (●).